High-pressure phases of $CaCO_3$: Crystal structure prediction and experiment

Artem R. Oganov [a,*], Colin W. Glass [a], Shigeaki Ono [b]

[a] *Laboratory of Crystallography, Department of Materials, ETH Hönggerberg, HCI G 515, Wolfgang-Pauli-Str. 10, CH-8093 Zurich, Switzerland*
[b] *Institute for Research on Earth Evolution, Japan Agency for Marine-Earth Science and Technology, 2-15 Natsushima-cho, Yokosuka-shi, Kanagawa 237-0061, Japan*

Abstract

Post-aragonite phase of $CaCO_3$, experimentally known to be stable above 40 GPa [S. Ono, T. Kikegawa, Y. Ohishi, J. Tsuchiya, Post-aragonite phase transformation in $CaCO_3$ at 40 GPa, Am. Mineral. 90 (2005) 667–671], is believed to be a major carbon-containing mineral in the Earth's mantle. Crystal structure of this mineral phase could not be solved using experimental data or traditional theoretical simulation methods and remained a controversial issue. Using a combination of advanced ab initio simulation techniques and high-pressure experiment, we have been able to determine the crystal structure of $CaCO_3$ post-aragonite. Here, we performed simulations with the USPEX code [C.W. Glass, A.R. Oganov, and N. Hansen, (in preparation). USPEX: a universal structure prediction program], which is based on an evolutionary algorithm using ab initio free energy as the fitness function. This novel methodology for crystal structure prediction, which uses only the chemical composition as input, is described in detail. For $CaCO_3$, we identify a number of energetically competitive structures, the most stable of which closely matches the experimental powder diffraction pattern and, in agreement with experiment, becomes more stable than aragonite above 42 GPa. This structure belongs to a new structure type, which is also adopted by the high-pressure post-aragonite phases of $SrCO_3$ and $BaCO_3$. It has 2 formula units in the orthorhombic unit cell (space group *Pmmn*) and contains triangular CO_3^{2-} ions and Ca^{2+} ions in the 12-fold coordination. Above 137 GPa, a pyroxene-type structure (space group $C222_1$) with chains of CO_4^{4-} tetrahedra becomes more stable than post-aragonite. For $MgCO_3$, this structure becomes more stable than magnesite above 106 GPa and is a good candidate structure for $MgCO_3$ post-magnesite.
© 2005 Elsevier B.V. All rights reserved.

Keywords: $CaCO_3$ post-aragonite; $MgCO_3$ post-magnesite; D″ layer; high pressure; crystal structure prediction; evolutionary algorithm; ab initio; density functional theory

1. Introduction

The fate of subducted carbonates has profound implications for the global carbon cycle in the Earth's system. The behavior of carbonates at high pressures and temperatures has been investigated by previous studies, because high-pressure polymorphs of carbonates could indeed be the host phases of carbon in the mantle. It is known that most dominant carbonates in the Earth are Mg- and Ca-bearing phases. Magnesite ($MgCO_3$), calcite ($CaCO_3$) and dolomite ($CaMg(CO_3)_2$) are the stable phases at ambient conditions. It was

reported that magnesite is stable at pressures corresponding to the upper and lower mantle [3]. The phase transition from calcite to aragonite occurs at upper mantle conditions (e.g., [4]). Dolomite breaks down into magnesite and aragonite at the uppermost part of the upper mantle [5–7]. Therefore, the high-pressure behaviour of magnesite and aragonite is important for the understanding of the geochemical cycle of carbon. Recently, a phase transition of magnesite was reported at pressures higher than 110 GPa by experimental and theoretical studies [8,9]. But the structure of this high-pressure phase is still an open question. In the case of $CaCO_3$, a pressure-induced phase transition of aragonite was observed, but the structure of post-aragonite remained a controversial issue. Santillán and Williams [10] reported that post-aragonite has a trigonal structure, which is the same as that of a high-pressure phase of $BaCO_3$ [11]. In contrast, Ono et al. [1] showed that post-aragonite has an orthorhombic structure. Therefore, it is necessary to investigate the structure of the post-aragonite phase in $CaCO_3$.

Recently, a new powerful methodology was developed, based on ab initio simulations and capable of predicting the most stable crystal structure for a given compound at given $P–T$ conditions [2,12]. Here we apply this methodology in order to clarify the structure of the post-aragonite phase in $CaCO_3$ at high pressures. We compare the predicted structure with the observed X-ray diffraction pattern of post-aragonite. Then, we discuss the structural properties and stability of $CaCO_3$ post-aragonite in the Earth's mantle and its transition to a pyroxene-type structure at 137 GPa, which sheds light on the nature of the post-magnesite transition of $MgCO_3$ [8].

2. Solving and predicting crystal structures from first principles

The basic principle determining the most stable crystal structure is simple: the stable structure has the lowest possible Gibbs free energy at given $P–T$ conditions. In spite of the simplicity of this principle, crystal structure prediction has been rated as one of the most difficult scientific problems [13]. The main difficulty is the overwhelmingly large multidimensional search space: even for systems with a small number of atoms in the unit cell, the number of possible different structures is astoundingly large. In fact, in all traditional simulation strategies, instead of trying all these structures, one starts with a list of expected crystal structure types (e.g., known for analogous systems), from which the

stable structure is identified with the help of simulations. This approach fails when a previously unknown or unexpected structure becomes stable (and such cases abound in literature), calling for a more systematic and rigorous approach to crystal structure prediction.

Recently, we have developed an ab initio evolutionary algorithm devised specifically for crystal structure prediction and implemented in the USPEX[1] code [1]. USPEX needs no prior information on the system and unlike previous attempts to use evolutionary algorithms for crystal structure prediction [14–16] utilizes ab initio free energies, rather than simple heuristic expressions, as the fitness function. Though computationally expensive, this allows us to address complex problems involving cases with unusual chemical bonding and electronic transitions. For certain types of rugged, high-dimensional search spaces, evolutionary algorithms have been shown to be a flexible and very powerful tool (see, e.g., [17]). By carefully tuning USPEX to the problem at hand, we have succeeded in greatly reducing the number of fitness function evaluations necessary to reach the global optimum compared with the algorithm of [14–16], rendering our ab initio evolutionary simulations very affordable and blessed with a much higher success rate, as shown by our numerous tests on various systems [12]. Additionally, this is the first evolutionary algorithm that is not limited to the case of fixed lattice parameters. This means that USPEX can predict new crystal structures in the absence of any experimental information. For details on USPEX, we refer the reader to [2]. For a review of the USPEX methodology and its first applications, see [12].

3. Computational methodology

Two types of evolutionary simulations were performed with USPEX: (1) using experimental unit cell parameters at 66.4 GPa [1] with 10 atoms in the unit cell and (2) variable-cell simulations at 50 GPa, 80 GPa and 150 GPa using no experimental information. In variable-cell simulations, we treated systems with 5, 10 and 20 atoms in the unit cell. Importantly, symmetry was not imposed in our calculations—instead, it was one of the results of the simulation; absence of symmetry constraints also ensures that all the produced structures are mechanically stable and do not contain soft Γ-point phonons. The first generation of structures was created randomly, the number of struc-

---

[1] Universal Structure Predictor: Evolutionary Xtallography.

tures in the population was $N+10$ (N is the number of atoms in the unit cell). Each generated structure was locally optimized using the conjugate-gradients method. The best 60% of each generation were used to produce the next-generation structures by heredity (90% structures) and permutation (10% structures)—the first being essential for exploiting the best aspects of all the good structures found, and the second being important for finding the best atomic ordering. For heredity, we represented atomic positions by real coordinates (not by the often used bit-strings), and the next-generation structure was obtained by combining the fractional coordinates of selected atoms from two parent structures; weighted-average heredity was adopted for the lattice vectors components. The best structure of the previous generation was set to survive and compete in the following generation. Typically, our global optimization runs required about 20 generations or less.

To calculate the fitness function of each produced structure, USPEX uses an external ab initio code—in present work, we used VASP [18]. Ab initio calculations performed here are based on the generalized gradient approximation [19] and the all-electron PAW method [20,21]. The PAW potentials used here were derived within the same generalized gradient approximation [19] and have [Ne] core (radius 2.3 a.u.) for Ca, [He] core (radius 1.5 a.u.) for C, [He] core (radius 1.52 a.u.) for O, and [Be] core (radius 2.0 a.u.) for Mg. As can be seen from Table 1, this level of theory is capable of reproducing experimental crystal structures and equations of state rather accurately. For known structures (calcite–Fig. 1a, aragonite–Fig.

1b) and for the best structure candidates produced by USPEX (Fig. 1c–g), we performed structure optimizations at a series of pressures between 0 and 100 GPa. In these calculations, we used the plane-wave cut-off of 600 eV, $8 \times 8 \times 8$, $6 \times 6 \times 6$ and $4 \times 4 \times 4$ meshes were used for Brillouin zone sampling of structures with 5, 10 and 20 atoms in the unit cell, respectively. Calculations proceeded self-consistently until the total energy converged to within 0.1 meV/cell, conjugate-gradients enthalpy minimization proceeded until the enthalpy changes became smaller than 1 meV/cell. For local optimization during evolutionary search, cruder (but still perfectly adequate) computational conditions were used: 450 eV cut-off; $4 \times 4 \times 4$, $4 \times 4 \times 4$ and $3 \times 3 \times 3$ Brillouin zone sampling for 5-, 10- and 20-atom systems, self-consistency tolerance of 0.2 meV/cell and structure relaxation tolerance of 2 meV/cell.

4. Results of fixed-cell evolutionary simulations: the post-aragonite structure

Fixed-cell simulations have been performed with experimental lattice parameters at 66.4 GPa reported in [1]: $a=4.101$ Å, $b=4.561$ Å, $c=3.964$ Å. Since it is the internal energy that is the relevant thermodynamic potential at constant volume and 0 K, these simulations searched for the lowest-energy structure. These simulations very readily gave the final structure reported in Table 2 and shown in Fig. 1c. The fact that simulations have arrived at a well-ordered, chemically meaningful and energetically favourable (as we will show below) structure supports the correctness of the

Table 1
Aragonite structure of CaCO$_3$

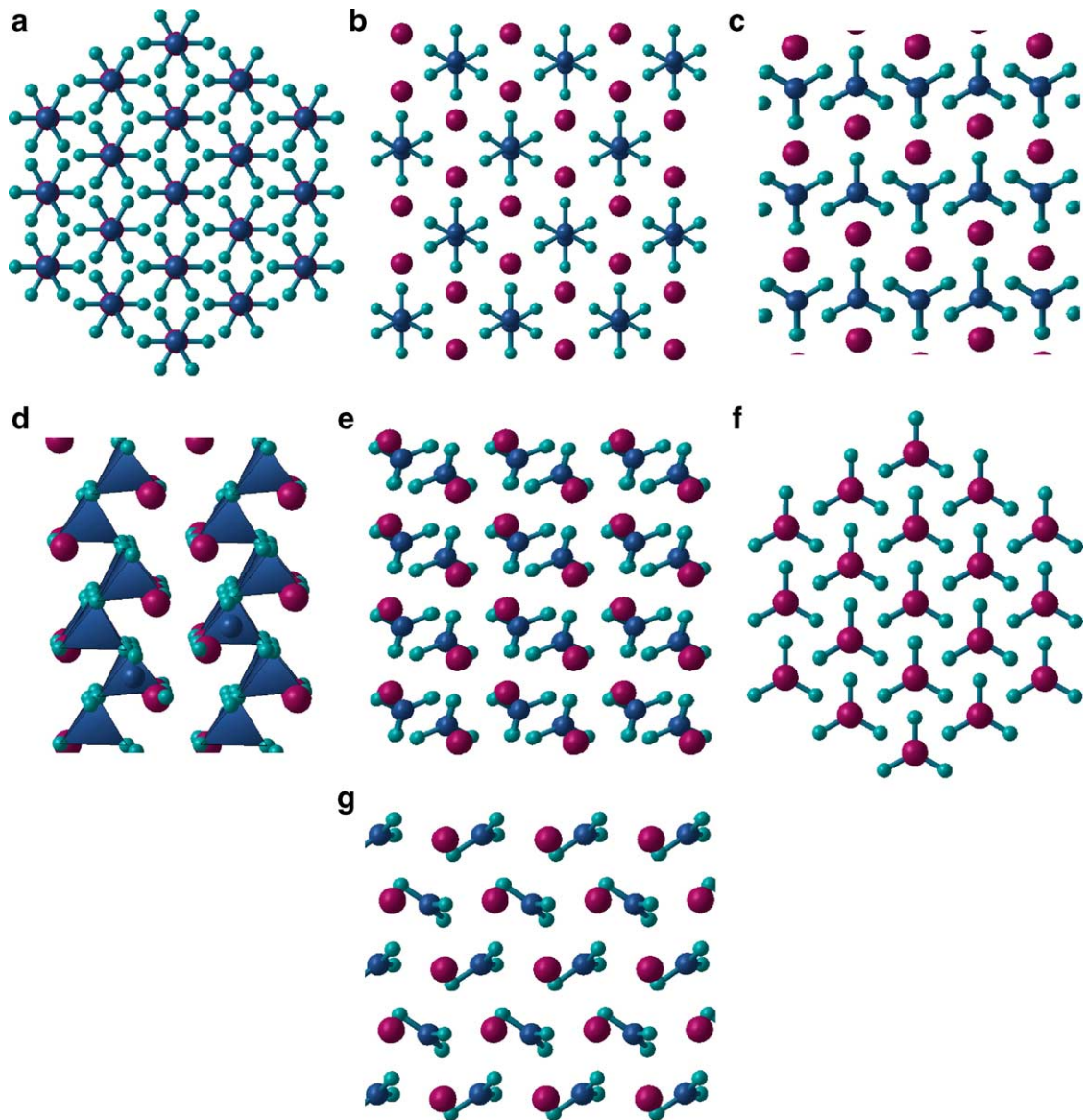| Parameters	Theory			Experiment [22]		
a (Å)	5.0192			4.9598		
b (Å)	8.0393			7.9641		
C (Å)	5.7952			5.7379		
V (Å^3)	233.84			226.65		
Atomic coordinates (space group $Pmcn$)						
Atoms	x	y	z	x	y	z
Ca	1/4	0.5859	0.2594	1/4	0.5851	0.2597
C	1/4	0.2377	0.4144	1/4	0.2386	0.4148
O1	1/4	0.0772	0.4043	1/4	0.0770	0.4043
O2	0.4738	0.3195	0.4126	0.4737	0.3196	0.4131
Bond lengths, Å	Ca–O1=2.440(x1), 2.684(x2)			Ca–O1=2.414(x1), 2.653(x2)		
	Ca–O2=2.473(x2), 2.538(x2), 2.576(x2)			Ca–O2=2.445(x2), 2.519(x2), 2.545(x2)		
	C–O1=1.292(x1); C–O2=1.3017(x2)			C–O1=1.288(x1); C–O2=1.284(x2)		
Third-order Birch–Murnaghan equation of state (fitted between 0 and 40 GPa)						
V_0 (Å^3)	233.84			226.65 [1]		
K_0 (GPa)	66.9			67.1 ± 6.3 [1]		
K'_0	4.48			4.7 ± 0.8 [1]		

Fig. 1. Crystal structures of CaCO$_3$: (a) calcite, (b) aragonite, (c) post-aragonite, (d) phase I, (e) phase II, (f) phase III, (g) phase IV. Large red spheres–Ca atoms; blue spheres–C atoms; green spheres–O atoms. (For interpretation of the references to colour in this figure legend, the reader is referred to the web version of this article.)

cell parameters of this phase derived in [1].[2] At fixed cell parameters, this structure is by far the most favourable one: the second best structure is 1.5 eV/cell higher in energy.

Fig. 2 shows a comparison between the experimental powder diffraction pattern of post-aragonite and the simulated diffraction pattern for the structure reported in Table 2. One can observe excellent agreement between these patterns, confirming our structure solution. Furthermore, as we show in Fig. 3, the new structure becomes more stable than aragonite above 42 GPa—in close agreement with experimental stability of post-aragonite above 40 GPa [1]. The calculated density discontinuity at the transition is 5.5%, close to the experimental estimate of ~5% [1]. The post-ara-

---

[2] We remind that experimental lattice parameters come from indexing of the diffraction pattern and as such can be non-unique and cannot be considered definitive if the structure of the material is not known. For example, the proposed [8] orthorhombic 30-atom cell for post-magnesite phase of MgCO$_3$ is likely incorrect: our simulations failed to give any energetically competitive structure at these cell parameters.

Table 2
Post-aragonite structure of CaCO$_3$ at several pressures

Parameters	66.4 GPa experimental cell			66.4 GPa theoretical cell			36 GPa experimental cell			36 GPa theoretical cell		
a (Å)	4.101			4.068			4.2802			4.3036		
b (Å)	4.561			4.592			4.6859			4.7248		
C (Å)	3.964			3.990			4.0613			4.0971		
V (Å^3)	74.145			74.534			81.456			83.309		
Atomic coordinates (pace group *Pmmn*)												
Atoms	x	y	z	x	y	z	x	y	z	x	y	z
Ca	0	1/2	0.6230	0	1/2	0.6220	0	1/2	0.6151	0	1/2	0.6162
C	0	0	0.9904	0	0	0.9902	0	0	0.9897	0	0	0.9900
O1	0	0	0.6700	0	0	0.6713	0	0	0.6742	0	0	0.6758
O2	0	0.2398	0.1473	0	0.2398	0.1474	0	0.2359	0.1429	0	0.2344	0.1421
Bond lengths (Å)	Ca–O1 = 2.288(x2), 2.357(x2) Ca–O2 = 2.228(x2), 2.393(x2), 2.496(x4) C–O1 = 1.270(x1) C–O2 = 1.258(x2)			Ca–O1 = 2.304(x2), 2.347(x2) Ca–O2 = 2.239(x2), 2.413(x2), 2.489(x4) C–O1 = 1.272(x1) C–O2 = 1.267(x2)			Ca–O1 = 2.355(x2), 2.441(x2) Ca–O2 = 2.282(x2), 2.475(x2), 2.602(x4) C–O1 = 1.281(x1) C–O2 = 1.269(x2)			Ca–O1 = 2.375(x2), 2.462(x2) Ca–O2 = 2.299(x2), 2.481(x2), 2.626(x4) C–O1 = 1.287(x1) C–O2 = 1.293(x2)		

gonite structure is characterized by the presence of 12-coordinate Ca atoms (in aragonite Ca is 9-coordinate) and can be viewed as hexagonal close packing of Ca^{2+} and O^{2-} ions with small C^{4+} ions in triangular voids.
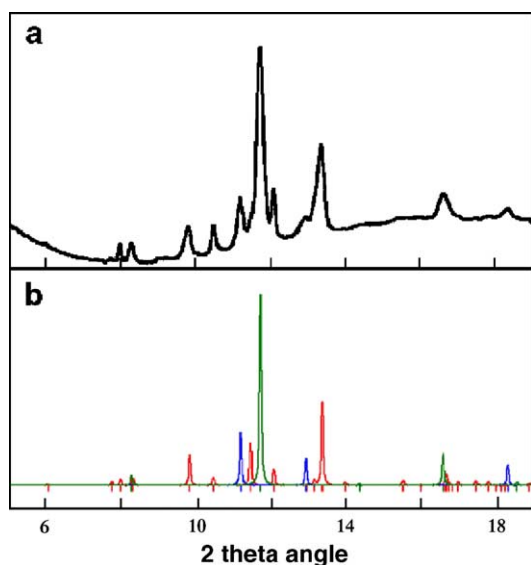

Fig. 2. Comparison of calculated and observed X-ray diffraction patterns of the post-aragonite phases. (a) observed X-ray diffraction pattern at 36 GPa and 300 K after laser heating (experimental details have been described elsewhere [1]). (b) Calculated X-ray diffraction pattern. Red, post-aragonite (*Pmmn*), a = 4.2802 Å, b = 4.6859 Å, and c = 4.0613 Å; blue, platinum (*Fm3m*), a = 3.7931 Å; green, B2-type sodium chloride (*Pm3m*), a = 2.9591 Å. Vertical bars indicate the calculated positions of the diffraction lines of each phase. (For interpretation of the references to colour in this figure legend, the reader is referred to the web version of this article.)

The third-order Birch–Murnaghan equation of state fitted to our results between 0 and 100 GPa yields the following parameters: V_0 = 109.74 Å^3, K_0 = 65.4 GPa, K_0' = 4.94. Since, for post-aragonite, no experimental data exist at low pressures, the zero-pressure parameters V_0, K_0 and K_0' determined from experiment are bound to suffer from large uncertainties, which are further enhanced by the strong correlation between these parameters. Refitting experimental data [1] with fixed K_0' = 4.94 yields V_0 = 101.8 ± 2.5 Å^3, K_0 = 90 ± 13 GPa; with fixed V_0 = 109.74 Å^3, we get K_0 = 42 ± 7 GPa, K_0' = 7.2 ± 1.2. Regardless of these uncertainties of parameterization, Table 2 shows that for post-aragonite, theoretical and experimental lattice parameters are in excellent agreement with each other.

5. Results of variable-cell evolutionary simulations: energetically competitive structures

Evolutionary variable-cell simulations with 5, 10, and 20 atoms in the unit cell were performed for three reasons. First, they allowed us to check if there are any energetically better structures—the conclusion being that the post-aragonite structure described above (which we also found in variable-cell simulations) is indeed the most stable structure at pressures between 42 GPa and 137 GPa, and we have found a new structure stable above 137 GPa. Second, these simulations showed that there are a large number of metastable, but energetically very competitive structures—these structures can in principle be obtained experimentally and their existence could explain the difference between experimental results obtained by
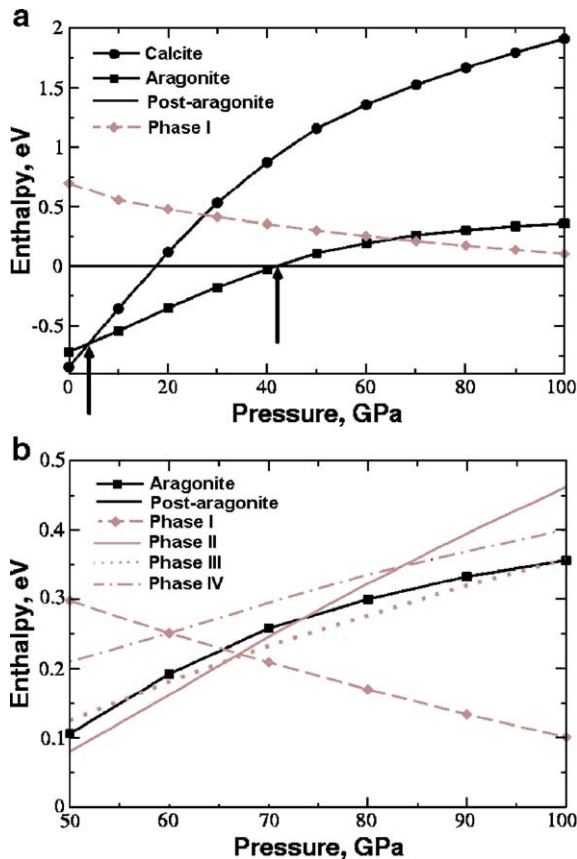
Fig. 3. Enthalpies (relative to post-aragonite) of candidate structures of $CaCO_3$ as a function of pressure. (a) From 0 GPa to 100 GPa showing stable phases (calcite, aragonite, post-aragonite) and phase I, which is stable above 137 GPa. Arrows indicate calcite–aragonite and aragonite–post-aragonite phase transitions at 4 GPa and 42 GPa, respectively. (b) Between 50 GPa and 100 GPa and showing also metastable phases II–IV. Enthalpies are calculated per formula unit, relative to post-aragonite. On compression to ~55 GPa aragonite spontaneously undergoes a metastable weakly first-order isosymmetric phase transition reversible on decompression to 25 GPa at zero Kelvin. Line "aragonite" in this figure at each pressure shows the lowest enthalpy for aragonite and its metastable isosymmetric polymorph.

different groups. Third, yielding a large number of energetically competitive structures, such simulations give a unique information on structural chemistry under pressure—we find that at 50 GPa, all such structures contain triangular CO_3^{2-} carbonate ions, whereas at 80 GPa, many structures also contained CO_4^{4-} tetrahedra (e.g., phase I—Fig. 1d), indicating that such structures become competitive well within the experimentally reachable pressure range. The most stable structure identified both at 50 GPa and 80 GPa is the already discussed post-aragonite structure, but several metastable structures turn out to be almost as stable in this pressure range.

Table 3
Theoretical structure of phase I of $CaCO_3$ (space group $C222_1$) at 150 GPa

Lattice parameters			
a (Å)	5.544		
b (Å)	6.926		
c (Å)	3.213		
V (Å³)	123.37		
Atomic coordinates (space group $C222_1$)			
Atoms	x	y	z
Ca	0	0.8287	1/4
C	0.3538	0	0
O1	0	0.3881	1/4
O2	0.2736	0.3875	0.7324
Bond lengths	Ca–O1 = 2.199(x2)		
(Å)	Ca–O2 = 2.036(x2), 2.123(x2), 2.132(x2), 2.333(x2)		
	C–O1 = 1.380(x2); C–O2 = 1.290(x2)		

Third-order Birch–Murnaghan equation of state (fitted between 0 and 200 GPa): $V_0 = 210.38$ Å³, $K_0 = 75.60$ GPa, $K'_0 = 4.84$.

Especially remarkable among our predicted structures is the orthorhombic (space group $C222_1$, 20 atoms in the conventional cell) pyroxene-type struc-
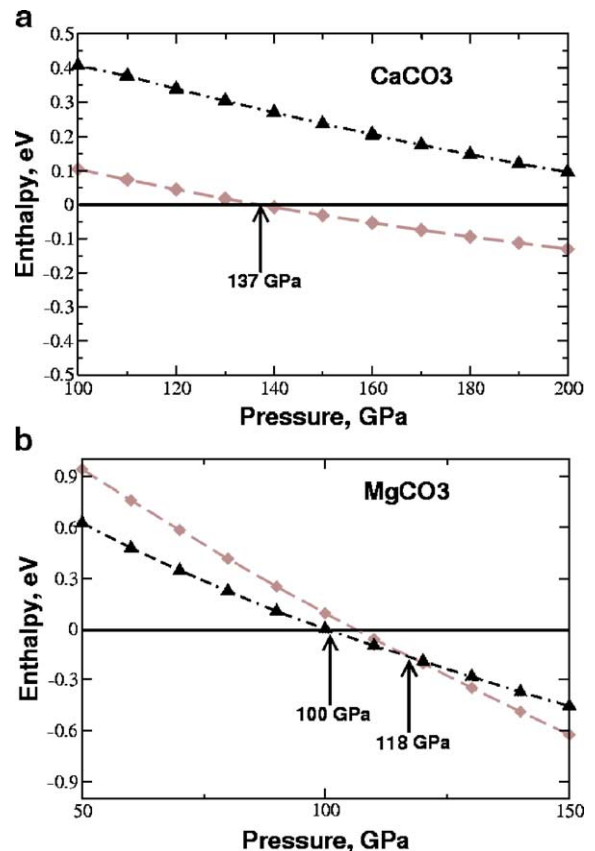

Fig. 4. Enthalpies of $C222_1$ (diamonds) and $C2/c$ (triangles) structures for (a) $CaCO_3$ (relative to post-aragonite) and (b) $MgCO_3$ (relative to magnesite) as a function of pressure. Results are given per formula unit.

ture I (Fig. 1d, Table 3), which is denser than any other structure discussed here. In our evolutionary simulations at 80 GPa, this structure appeared as metastable, but in simulations at 150 GPa it came up as the most stable, in agreement with our static enthalpy-minimisation calculations which show it to be more stable than post-aragonite above 137 GPa. Thus, we find the limits for the enormous stability field of post-aragonite: 42–137 GPa. Additionally, we find energetically competitive but always metastable phases II (triclinic, space group $P\bar{1}$, 10 atoms in the unit cell), III (trigonal, space group $R3m$, 5 atoms in the rhombohedral cell), IV (monoclinic, space group $P2_1$, 10 atoms in the cell)—all containing carbon only in the form of CO_3^{2-} ions. Phases II–IV have densities similar to that of aragonite and are less dense than post-aragonite and phase I. With the exception of a less stable phase IV, all the other CO_3^{2-} ion-containing structures (calcite, aragonite, post-aragonite, phase II, phase III) have CO_3^{2-} ions in a parallel orientation. This is a typical feature of carbonate crystal structures, determining strong anisotropy of their physical properties (e.g., famous birefringence of calcite).

6. Stability of the $C222_1$ structure for $CaCO_3$ and $MgCO_3$: insights into the post-magnesite transition of $MgCO_3$

Our static calculations (Fig. 4a) show that for $CaCO_3$ phase I ($C222_1$) becomes more stable than post-aragonite at 137.2 GPa. The density discontinuity at this transition is rather small, 1.25%.

We have decided to check whether the same structure could be adopted by the post-magnesite phase of

Table 4
Theoretical structure of the candidate post-magnesite phase (space group $C222_1$) of $MgCO_3$ at 120 GPa

Lattice parameters			
a (Å)	5.552		
b (Å)	7.201		
c (Å)	2.880		
V (Å^3)	115.14		
Atomic coordinates (space group $C222_1$)			
Atoms	x	y	z
Mg	0	0.8049	1/4
C	0.3355	0	0
O1	0	0.3930	1/4
O2	0.2907	0.3801	0.7252
Bond lengths	Mg–O1 = 2.026(x2)		
(Å)	Mg–O2 = 1.875(x2), 1.982(x2), 2.094(x2), 2.549(x2)		
	C–O1 = 1.395(x2); C–O2 = 1.287(x2)		

Third-order Birch–Murnaghan equation of state (fitted between 0 and 150 GPa): V_0 = 182.64 Å^3, K_0 = 77.64 GPa, K_0' = 5.18.

$MgCO_3$. We find that the *Pmmn* post-aragonite structure is not stable for $MgCO_3$. Our calculations show (Fig. 4b) that for $MgCO_3$, the $C2/c$ structure of Skorodumova et al. [9] becomes more stable than magnesite above 100.3 GPa, but is less stable than our $C222_1$ structure above 117.7 GPa. Both structures contain zigzag chains of corner-sharing CO_4^{4-} tetrahedra and are energetically close. Transition from magnesite to the $C2/c$ structure is accompanied by a density jump of 5.2%, the density jump for the $C2/c$–$C222_1$ transition is 2.8%. The optimized structure and the equation of state of the $C222_1$ phase at 120 GPa are given in Table 4. To clarify whether or not the $C2/m$ and $C222_1$ structures actually correspond to global minima of the free energy, we plan to run evolutionary simulations for $MgCO_3$ under pressure. In any case, it seems likely that the stable post-magnesite phase(s) will be based on tetrahedral carbonate chains, like both $C222_1$ and $C2/c$ structures.

7. High-pressure crystal chemistry of carbonates: rationalisation

Based on this work and experiments [25], the sequence of pressure-induced phase transitions in MCO_3 carbonates (M = Mg, Ca, Sr)[3] is given in Table 5. One can see a somewhat surprising difference between $MgCO_3$ and $CaCO_3$. At the same time, $CaCO_3$, $BaCO_3$ and $SrCO_3$ behave in similar ways.[4] All these trends are easily explained by the sizes of the cations: Mg^{2+} is rather small, and therefore, $MgCO_3$ cannot adopt the aragonite and post-aragonite structures, where Mg^{2+} would be 9- and 12-coordinate, respectively. Instead of adopting these structures, $MgCO_3$ "skips" them and transforms directly into the $C2/c$ and $C222_1$ structures with tetrahedral carbonate ions;[5] the further transition from $C2/c$ to $C222_1$ is accompanied by an increase of the coordination number of Mg^{2+}. An overall increase of coordination numbers with pressure enables more efficient packing of the atoms and is related to the increase of the cation/anion radius ratio under pressure.

For $CaCO_3$, $SrCO_3$ and $BaCO_3$ the situation is different: the size of Ca^{2+} is on the border between 6- and

---

[3] $BaCO_3$ is less well studied, but seems to be a perfect analogue of $SrCO_3$.
[4] Except that for $SrCO_3$ and $BaCO_3$, the calcite structure is not stable, since Sr^{2+} and Ba^{2+} are too large to occupy octahedral positions in that structure.
[5] We note, however, that this sequence of phase transitions in $MgCO_3$ is tentative and has to be assessed by future evolutionary simulations of $MgCO_3$.

Table 5
Summary of the high-pressure phases of $MgCO_3$, $CaCO_3$ and $SrCO_3$

Cation radius increases ↓	Pressure increases →				
	Compounds	Structure types			
		Calcite CN(C)=3 CN(M)=6	Aragonite CN(C)=3 CN(M)=9	Post-aragonite CN(C)=3 CN(M)=12	$C2/c$ pyroxene CN(C)=4 CN(M1)=6 CN(M2)=8	$C222_1$ CN(C)=4 CN(M)=10
	$MgCO_3$	0–100 GPa	–	–	(100–118 GPa)	(>118 GPa)
	$CaCO_3$	0–4 GPa	4–42 GPa	42–137 GPa	–	>137 GPa
	$SrCO_3$	–	0–10 GPa	>10 GPa	(unstable?)	(stable?)

"CN" denotes coordination numbers of cations in structure types.

9-fold coordination, and therefore, $CaCO_3$ transforms from calcite with CN(Ca)=6 into aragonite with CN(Ca)=9 at rather low pressures. On further increase of pressure, aragonite-type $CaCO_3$, $SrCO_3$ and $BaCO_3$ transform into the post-aragonite *Pmmn* structures with cations in the 12-fold coordination. The post-aragonite structure is rather dense and is based on the hexagonal close packing of Ca^{2+} and O^{2-} ions, which explains its enormous stability field. From the post-aragonite structure, these carbonates transform into the $C222_1$ structure with the tetrahedral carbonate ions and Ca^{2+} in the 10-fold coordination. The $C2/c$ structure is not stable[6], because 6- and 8-fold coordination sites of this structure are too small to accommodate large Ca^{2+}, Sr^{2+} and Ba^{2+} cations.

8. Discussion

Theory and experiment can fruitfully complement each other in the search for new high-pressure phases [23,24]. However, severe limitations existed on the theoretical side: calculations could only be performed starting with some list of expected structure types, thus almost completely excluding the possibility of finding new structure types by standard simulations. With the methodology presented here, this limitation can be lifted. In this work, a new stable crystal structure type was derived purely on the basis of theory.

This is the first application of the USPEX methodology [2,12] for the prediction of hitherto unknown crystal structures. It demonstrates the full power of this approach—i.e., the successful prediction of the stable crystal structure, as well as of a number of robust metastable structures. This allows one to explore the

phase diagram of any material without experimental input and "scan" the chemistry of a given compound by looking at good metastable, as well as stable, structures (which is invaluable for understanding the reasons of stability of certain structures and the dominant stabilizing or destabilizing interactions and can be used to establish rules determining stable crystal structures).

Here we have found a novel stable (between 42 GPa and 137 GPa) structure for $CaCO_3$, which could not be solved experimentally [1]; this structure perfectly matches the experimental powder diffraction pattern, stability field and density of the post-aragonite phase [1]. Due to the wide stability field of this phase and abundance of Ca in the Earth, this dense phase is likely to be a major mineral of carbon in the Earth's lower mantle, together with $MgCO_3$ magnesite [3] and post-magnesite [8]. The greater density of post-aragonite compared with aragonite is achieved due to the higher coordination of Ca (12-fold instead of 9-fold in aragonite). Stability conditions of $CaCO_3$ post-aragonite correspond to depths greater than 1000 km. The post-aragonite structure found here matches the diffraction pattern of the high-pressure phase of $SrCO_3$ [25] and $BaCO_3$ (Ono et al., unpublished), but not of the unsolved structure of $MgCO_3$ post-magnesite [8].

Our simulations showed that triangular CO_3^{2-} ions are remarkably stable under pressure: all energetically good $CaCO_3$ structures obtained at 50 GPa contained these ions. In all of these structures (except one, which was the least stable) the arrangement of the CO_3^{2-} ions was parallel; this is characteristic of all the stable carbonate structures (however, metastable $CaCO_3$ vaterite deviates from it) and could be favoured due to better packing density and/or minimized repulsions between the carbonate groups. Parallel alignment of the CO_3^{2-} groups in carbonate structures determines the strong anisotropy of their physical properties, e.g., anisotropic compressibility and optical birefringence. CO_4^{4-} tetrahedra, appearing in energetically competitive structures

---

[6] We note that starting with the $C2/c$ structure, after structure optimization for $CaCO_3$ we obtained a higher symmetry (*Cmca*) structure with Ca in the 12-fold coordination (in $C2/c$ $MgCO_3$ half of the Mg atoms are in 6-fold and half in the 8-fold coordination).

at 80 GPa, indicate a crossover to an altogether new crystal-chemical regime. An orthorhombic (space group $C222_1$) pyroxene-type structure containing chains of corner-linked CO_4^{4-} tetrahedra is predicted in our simulations to become more stable than post-aragonite at 137 GPa and might in fact be present at the very bottom of the Earth's D″ layer ($P < 136$ GPa) if stabilized by temperature and/or impurities.

We have demonstrated that the $C222_1$ structure could also be the structure of $MgCO_3$ post-magnesite, experimentally found above 115 GPa [8]. We find that this structure is energetically close to the structure proposed by Skorodumova et al. [9] for the post-magnesite phase of $MgCO_3$ and becomes more stable than that structure [9] above 118 GPa. While further work is needed to elucidate the structure of $MgCO_3$ post-magnesite, it is likely to be a pyroxene-type structure containing tetrahedral carbonate ions. The formation of such structures in $CaCO_3$ and $MgCO_3$ under pressure indicates a major change in the crystal chemistry of carbonates within the Earth's lowermost mantle.

Acknowledgments

References

[1] S. Ono, T. Kikegawa, Y. Ohishi, J. Tsuchiya, Post-aragonite phase transformation in $CaCO_3$ at 40 GPa, Am. Mineral. 90 (2005) 667–671.

[2] C.W Glass, A.R. Oganov, and N. Hansen. USPEX: a universal structure prediction program (in preparation).

[3] G. Fiquet, F. Guyot, M. Kunz, J. Matas, D. Andrault, M. Hanfland, Structural refinements of magnesite at very high pressure, Am. Mineral. 87 (2002) 1261–1265.

[4] K. Suito, J. Namba, T. Horikawa, Y. Taniguchi, N. Sakurai, M. Kobayashi, A. Onodera, O. Shimomura, T. Kikegawa, Phase relations of $CaCO_3$ at high pressure and high temperature, Am. Mineral. 86 (2001) 997–1002.

[5] I. Martinez, J. Zhang, R.J. Reeder, In situ X-ray diffraction of aragonite and dolomite at high pressure and high temperature: evidence for dolomite breakdown to aragonite and magnesite, Am. Mineral. 81 (1996) 611–624.

[6] K. Sato, T. Katsura, Experimental investigation on dolomite dissociation into aragonite–magnesite up to 8.5 GPa, Earth Planet. Sci. Lett. 184 (2001) 529–534.

[7] M. Shirasaka, E. Takahashi, Y. Nishihara, K. Matsukage, T. Kikegawa, In situ X-ray observation of the reaction dolomite = aragonite + magnesite at 900–1300 K, Am. Mineral. 87 (2002) 922–930.

[8] M. Isshiki, T. Irifune, K. Hirose, S. Ono, Y. Ohishi, T. Watanuki, E. Nishibori, M. Takadda, M. Sakata, Stability of magnesite and its high-pressure form in the lowermost mantle, Nature 427 (2004) 60–63.

[9] N.V. Skorodumova, A.B. Belonoshko, L. Huang, R. Ahuja, B. Johansson, Stability of the $MgCO_3$ structures under lower mantle conditions, Am. Mineral. 90 (2005) 1008–1011.

[10] J. Santillán, Q. Williams, A high pressure X-ray diffraction study of aragonite and the post-aragonite phase transition in $CaCO_3$, Am. Mineral. 89 (2004) 1348–1352.

[11] C.M. Holl, J.R. Smyth, H.M.S. Laustsen, S.D. Jacobsen, R.T. Downs, Compression of witherite to 8 GPa and the crystal structure of $BaCO_3$—II, Phys. Chem. Miner. 27 (2000) 467–473.

[12] A.R Oganov, and C.W. Glass. Crystal structure prediction using ab initio evolutionary techniques: principles and applications (in preparation).

[13] J. Maddox, Crystals from first principles, Nature 335 (1988) 201.

[14] T.S. Bush, C.R.A. Catlow, P.D. Battle, Evolutionary programming techniques for predicting inorganic crystal structures, J. Mater. Chem. 5 (1995) 1269–1272.

[15] S.M. Woodley, P.D. Battle, J.D. Gale, C.R.A. Catlow, The prediction of inorganic crystal structures using a genetic algorithm and energy minimization, Phys. Chem. Chem. Phys. 1 (1999) 2535–2542.

[16] S.M. Woodley, Prediction of crystal structures using evolutionary algorithms and related techniques, Struct. Bond. 110 (2004) 95–132.

[17] Z. Michalewicz, D.B. Fogel, How to Solve It: Modern Heuristics, Springer, Berlin, 2004.

[18] G. Kresse, J. Furthmüller, Efficient iterative schemes for ab initio total-energy calculations using a plane wave basis set, Phys. Rev. B54 (1996) 11169–11186.

[19] J.P. Perdew, K. Burke, M. Ernzerhof, Generalized gradient approximation made simple, Phys. Rev. Lett. 77 (1996) 3865–3868.

[20] P.E. Blöchl, Projector augmented-wave method, Phys. Rev. B50 (1994) 17953–17979.

[21] G. Kresse, D. Joubert, From ultrasoft pseudopotentials to the projector augmented-wave method, Phys. Rev. B59 (1999) 1758–1775.

[22] B. Dickens, J.S. Bowen, Refinement of the crystal structure of the aragonite phase of $CaCO_3$, J. Res. Natl. Bur. Stand., A Phys. Chem. 75 (1971) 27–32.

[23] A.R. Oganov, S. Ono, Theoretical and experimental evidence for a post-perovskite phase of $MgSiO_3$ in Earth's D″ layer, Nature 430 (2004) 445–448.

[24] A.R. Oganov, S. Ono, The high pressure phase of alumina and implications for Earth's D″ layer, Proc. Natl. Acad. Sci. 102 (2005) 10828–10831.

[25] S. Ono, M. Shirasaka, T. Kikegawa, Y. Ohishi, A new high-pressure phase of strontium carbonate, Phys. Chem. Miner. 32 (2005) 8–12.